

Identification of LOFA precursors in ITER superconducting magnet cryogenic cooling circuit

Original

Identification of LOFA precursors in ITER superconducting magnet cryogenic cooling circuit / Destino, Vincenzo; Bonifetto, Roberto; Di Maio, Francesco; Pedroni, Nicola; Zanino, Roberto; Zio, Enrico. - In: RELIABILITY ENGINEERING & SYSTEM SAFETY. - ISSN 0951-8320. - ELETTRONICO. - 209:(2021), p. 107426. [10.1016/j.ress.2020.107426]

Availability:

This version is available at: 11583/2915874 since: 2021-07-29T14:36:49Z

Publisher:

Elsevier Ltd

Published

DOI:10.1016/j.ress.2020.107426

Terms of use:

This article is made available under terms and conditions as specified in the corresponding bibliographic description in the repository

Publisher copyright

Elsevier postprint/Author's Accepted Manuscript

© 2021. This manuscript version is made available under the CC-BY-NC-ND 4.0 license
<http://creativecommons.org/licenses/by-nc-nd/4.0/>. The final authenticated version is available online at:
<http://dx.doi.org/10.1016/j.ress.2020.107426>

(Article begins on next page)

Identification of LOFA Precursors in ITER Superconducting Magnet Cryogenic Cooling Circuit

V. Destino¹, R. Bonifetto¹, F. Di Maio², N. Pedroni¹, R. Zanino¹, E. Zio^{2,3,4}

¹ *NEMO group, Dipartimento Energia, Politecnico di Torino, Torino, Italy*

² *Dipartimento di Energia, Politecnico di Milano, Italy*

³ *MINES ParisTech, PSL Research University, CRC, Sophia Antipolis, France*

⁴ *Eminent scholar at Kyung Hee University, Republic of Korea*

ABSTRACT: In the International Thermonuclear Experimental Reactor, plasma is magnetically confined with Superconductive Magnets (SMs) that must be maintained at cryogenic temperature by a Superconducting Magnet Cryogenic Cooling Circuit (SMCCC). To guarantee cooling, Loss-Of-Flow Accidents (LOFAs) in the SMCCC are to be avoided. In this work, an approach to identify LOFA precursors (i.e., those component failures leading to a LOFA) is presented. The approach is based on a Spectral Clustering (SC) method using the Fuzzy C-Means (FCM) algorithm and is applied to the SMCCC of a single module of the ITER Central Solenoid (CS).

KEY WORDS: Nuclear Fusion, ITER, Superconducting Magnets, Cryogenic Cooling Circuit, Loss-Of-Flow Accident (LOFA), Precursors, Spectral Clustering, Fuzzy C-Means

List of Acronyms

B	Burning	LOFA	Loss-Of-Flow Accident
BV	By-pass Valve	M	Last Magnetization
C1	Control system 1	MVL	Multiple Valued Logic
C2	Control system 2	NC	Normally Closed
CC	Correction Coil	NO	Normally Open
CP	Centrifugal Pump	OSSC	On-line Supervised Spectral Clustering
CS	Central Solenoid	PF	Poloidal Field
CSM	Central Solenoid Module	QT	Quench Tank
CV	Control Valve	R	Rump Down
D	Dwell	SC	Spectral Clustering
FCM	Fuzzy C-Means	SHe	Supercritical Helium
FM	First Magnetization	SM	Superconductive Magnet
HX	Heat exchanger	SMCCC	Superconducting Magnet Cryogenic Cooling Circuit
ITER	International Thermonuclear Experimental Reactor	SV	Safety Valve
LHe	Liquid Helium	TF	Toroidal Field

List of Symbols

G_0	Nominal flow in the CSM	$t_{LOFA,C1,i}$	Time of LOFA detection by C1 at i -th scenario
I/I_{cr}	Current to critical current in the CSM		
$(I/I_{cr})_{lim}$	Limit value of I/I_{cr}	$x_j^k(t)$	k -th variable trend of j -th scenario
p_0	CP downstream pressure	x_{il}^k	Value of $x_i^k(t)$ at l -th time
p_{QT}	QT pressure	x_{jl}^k	Value of $x_j^k(t)$ at l -th time
p_{lim}	Pressure limit in the CSM	\bar{X}^k	Matrix containing each x_{il}^k at i -th row and l -th column
p_{max}	Rupture pressure of the CSM		
$p_{CSM,in}$	Inlet pressure in the CSM	y_{il}^k	Normalization of x_{il}^k
T_{QT}	Temperature in the QT	y_{jl}^k	Normalization of x_{jl}^k
T_{cs}	Current sharing temperature	δ_{ij}	Euclidean pointwise distance between an i -th scenario and a j -th scenario from $l = 1$ to $l = L$
T_{hs}	Hotspot temperature		
T_{sat}	LHe temperature		
ΔV	Electric potential of the CSM	$\delta_{l,ji}$	Euclidean pointwise distance between a j -th scenario and a i -th scenario from $p = 1$ to $p = l$
ΔV_{lim}	Limit value of ΔV		
m_{CP}	Failure magnitude of CP	F	Coefficient for similarity calculation
m_{CV1}	Failure magnitude of CV1	α, β	Parameters for F calculation
m_{CV2}	Failure magnitude of CV2	\bar{W}	Similarity matrix
m_{BV}	Failure magnitude of BV	\bar{W}_i	Generic i -th row of \bar{W}
m_{SV1}	Failure magnitude of SV1	w_{ij}	Generic element of \bar{W} at i -th row and j -th column
m_{SV2}	Failure magnitude of SV2		
t_{CP}	Failure time of CP	$\bar{W}_{l,j}$	Similarity vector of a j -th scenario with training scenarios at l -th time
t_{CV1}	Failure time of CV1		
t_{CV2}	Failure time of CV2		
t_{BV}	Failure time of BV	$w_{l,ji}$	Similarity between a j -th scenario and an i -th scenario at l -th time
t_{SV1}	Failure time of SV1		
t_{SV2}	Failure time of SV2	d_i	Sum of all elements in \bar{W}_i
ord_{CP}	Failure order of CP	$d_{l,j}$	Sum of all elements in $\bar{W}_{l,j}$
ord_{CV1}	Failure order of CV1	\bar{D}	Degree matrix
ord_{CV2}	Failure order of CV2	\bar{L}	Laplacian Matrix
ord_{BV}	Failure order of BV	\bar{L}_{sym}	Normalized Laplacian Matrix
ord_{SV1}	Failure order of SV1	λ_c	Generic c -th eigenvalue of \bar{L}_{sym}
ord_{SV2}	Failure order of SV2	\vec{u}_c	Eigenvector of \bar{L}_{sym} associated to λ_c
t_{miss}	Mission time	\bar{P}_c	Generic c -th vector obtained from \bar{D} matrix and \vec{u}_c vector
τ_{val}	Validation time of control systems		
i	Accidental training scenario	\bar{U}	Matrix containing each \vec{u}_c element
j	Accidental scenario	\bar{U}_i	Vector with the generic i -th row of \bar{U}
k	Variable index	u_{ic}	Generic c -th element of \bar{U}_i
l, p	Time indexes	$\bar{U}_{l,j}$	Vector with eigenspace coordinates related to $\bar{W}_{l,j}$
c, h	Cluster indexes		
Δt	Time step	$u_{l,jc}$	Generic c -th element of $\bar{U}_{l,j}$
N_{train}	Number of training scenarios	\bar{T}	Normalization of \bar{U}
N_{test}	Number of testing scenarios	\bar{T}_i	Vector with the generic i -th row of \bar{T}
Z	Number of variables monitored	t_{ic}	Generic c -th element of \bar{T}
L	Total number of time points	$\bar{T}_{l,j}$	Normalization of $\bar{U}_{l,j}$
C	Number of clusters	$t_{l,jc}$	Generic c -th element of $\bar{T}_{l,j}$
$x_i^k(t)$	k -th variable trend of i -th scenario	ρ	Fuzzy partition exponent

J_m	Objective function of FCM	\mathcal{F}_{ce}	Generic element of $\bar{\bar{\mathcal{F}}}$ referring to c -th cluster and e -th component
\bar{A}_c	Vector with eigenspace coordinates of the c -th centre	E	Number of components in $\bar{\bar{\mathcal{F}}}$
$\bar{\bar{A}}$	Matrix containing \bar{A}_c at each c -th row	$V_{lim,LOFA,l}$	Limit for LOFA precursors identification at l -th time
a_{ch}	Generic h -th element of \bar{A}_c	V_{1st}	First highest $V_{rel,l,cj}$ at l -th time
M_{ci}	Membership of the i -th scenario to the c -th cluster	V_{2nd}	Second highest $V_{rel,l,cj}$ at l -th time
M_{lim}	Membership limit for clustering	c_{1st}	Cluster associated to V_{1st}
$\bar{\bar{M}}$	Matrix containing M_{ci} at c -th row and i -th column	c_{2nd}	Cluster associated to V_{2nd}
$M_{l,cj}$	Membership of j -th scenario to c -th cluster at l -th time	$Flag_{LOFA}$	Flag for LOFA precursors identification
$M_{l,c0}$	Membership of a scenario with no failures to c -th cluster at l -th time	$t_{last,Fail,i}$	Time of last component failure before $t_{LOFA,C1,i}$
$M_{rel,l,cj}$	Difference between $M_{l,cj}$ and $M_{l,c0}$	$t_{lim,i}$	Average between $t_{last,Fail,i}$ and $t_{LOFA,C1,i}$
$V_{rel,l,cj}$	Difference quotient of $M_{rel,l,cj}$	$V_{lim,i}$	Second highest $V_{rel,l,ci}$ at $t_{lim,i}$
q	Index of the current phase	$M_{lim,FAIL,l}$	Limit for component precursors identification at l -th time
$\bar{\bar{L}}$	LOFA map	$Flag_{FAIL,e}$	Flag for e -th component failure
\mathcal{L}_{cq}	Generic element of $\bar{\bar{L}}$ referring to the c -th cluster and q -th phase	$Count_{FAIL,e}$	Number of $M_{rel,l,cj}$ that overcome $M_{lim,FAIL,l}$ at l -th time
Q	Number of current phases	S	Proportional constant between l -th time and $M_{lim,FAIL,l}$
e	Component index		
$\bar{\bar{\mathcal{F}}}$	Map with prototypical failures		

1. INTRODUCTION

ITER (International Thermonuclear Experimental Reactor) (2018) will be the first reactor to produce a net amount of energy exploiting fusion reactions between Deuterium and Tritium. The reactor is a tokamak in which the plasma is magnetically confined in a torus chamber by different Superconductive Magnets (SMs) (Bigot, 2018): one Central Solenoid coil (CS), eighteen Toroidal Field coils (TFs), six Poloidal Field coils (PFs) and eighteen Correction Coils (CCs). The CS is constituted by six Central Solenoid Modules (CSMs). Each CSM must sustain high currents (~ 40 kA) in order to generate high magnetic fields (several T) to confine the plasma and its superconductive properties must be guaranteed to nullify ohmic heating (Takahashi et al., 2006). The CSMs are cooled with Supercritical Helium (SHe) at 4.5 K with a pressure of 0.5-0.6 MPa (Mitchell et al., 2008) by a Superconducting Magnet Cryogenic Cooling Circuit (SMCCC) that is in charge of the extraction of the heat from the CSMs and its transfer to pools of saturated Liquid Helium (LHe) (Zanino et al., 2010).

A Loss-Of-Flow Accident (LOFA) in the SMCCC is of major concern because it can impair the CS cooling capability, possibly leading to rapid surge of the CS pressure and temperature due to the ohmic heating. If the pressure and the temperature overcome 25 MPa and 150 K, respectively, the CS could be lost (IAEA, 2002; ITER, 2006; Wu et al., 2016; Savoldi et al., 2018; Bellaera et al., 2020).

In this work, we present an automatic data-driven approach which is representative of plant conditions that may lead to failure of SMCCC components that are precursors of a LOFA. The approach is based on On-line Supervised Spectral Clustering (OSSC) that uses the Fuzzy C-Means (FCM) algorithm to recognise those patterns of measured signals (Baraldi et al., 2015; Di Maio et al., 2016; Al-Dahidi et al., 2018).

The remainder of the paper is organized as follows. In Section 2, a description of the SMCCC, the CS and the deterministic code 4C (Savoldi et al., 2010) used to simulate one of the six CSMs is provided. In Section 3, the information used for developing the approach to LOFA precursors identification is presented. In Section 4, the LOFA precursors identification approach is presented. It is, then, tested in Section 5 on the CSM of Section 2. Finally, a brief summary of the work and some conclusions are reported in Section 6.

2. THE SUPERCONDUCTING MAGNET CRYOGENIC COOLING CIRCUIT (SMCCC)

The SMCCC cools down the six CSMs with Supercritical Helium (SHe) (Savoldi et al., 2014). Fig.1 sketches a simplified scheme of the circuit, where only one CSM is connected with the cooling system. The Centrifugal Pump (CP) keeps the coolant in motion in the two cryolines, guaranteeing a nominal flow $G_0 = 0.32 \text{ kg/s}$ and a downstream pressure $p_0 = 0.42 \text{ MPa}$ at nominal operational conditions (Savoldi et al., 2014; Bellaera et al., 2020). The heat exchanger HX2 removes the heat produced in the CSM, while the HX1 cools the SHe after the compression in the CP with Liquid Helium (LHe) at saturated conditions ($T_{sat} = 4.5 \text{ K}$). The Control Valves (CV1 and CV2) are Normally Open (NO) during nominal operational conditions, whereas the two Safety Valves (SV1 and SV2) and the By-pass Valve (BV) are Normally Closed (NC). The controllers C1 and C2 receive signals from the flow meters and pressure detectors, respectively, and use them to actuate the components for flow control.

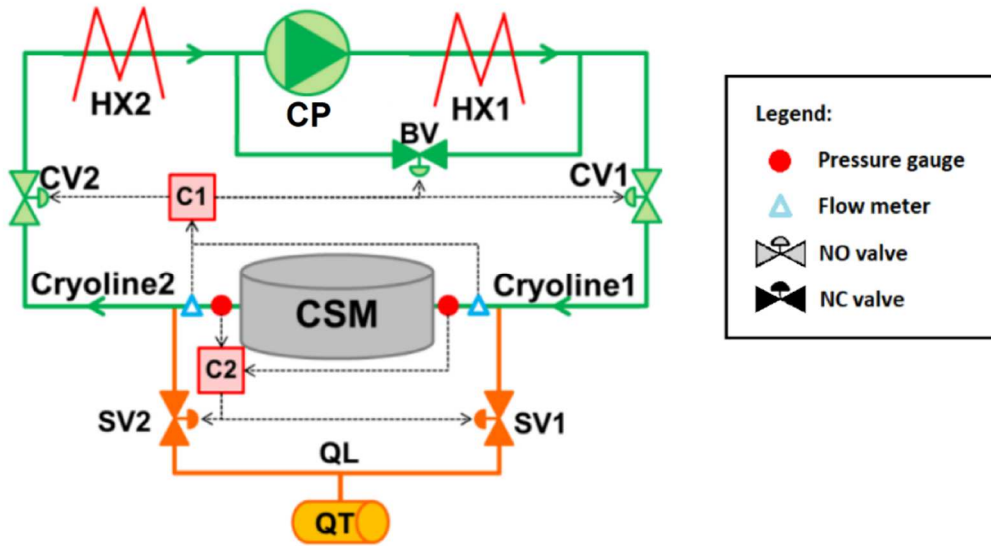


Figure 1 Simplified SMCCC (adapted from Bellaera et al., 2020)

In case of occurrence of a LOFA, when the coolant flow goes below 10% of the nominal value for more than the validation time ($\tau_{val} = 1s$) both at the CSM inlet and the CSM outlet (Savoldi et al., 2018):

- C1 closes CV1 and CV2, opens BV to prevent CP failure and dumps the current inside the CSM in 30s (ITER, 2014); in this way, SHe flows only through the by-pass line, so that the CSM is isolated and the inventory of bi-phase helium upstream of the CP is reduced.
- C2 opens the two SVs when the pressure in the CSM goes beyond $p_{lim} = 1.8 MPa$, sending SHe in the Quench Tank (QT) at pressure $p_{QT} = 0.35 MPa$ and temperature $T_{QT} = 300 K$ (Bellaera et al., 2020), so as to avoid reaching pressures above $p_{max} = 25 MPa$ (which is the design criterion to ensure pressure integrity of the CSM during quenching) (ITER, 2009).

The cooling circuit behaviour has been simulated for a mission time $t_{miss} = 3600s$ with the *Cryogenic Circuit Conductor and Coil code* (4C code) that integrates (Savoldi et al., 2010):

- a 1-D thermal-hydraulic model for each channel of the CSM;
- a 2^{1/2}-D model based on Freefrem++ to account for heat conduction phenomena in each radial section of the CSM;
- a 1-D compressible fluid model (for pipes and HXs) based on Dymola;
- a 0-D model for the mass and the energy balances, in relevant points of the cooling loop (such as valves, QT, pump, ...).

For each i -th simulation, the following set of Z variables $x_i^k(t)$ [$k = 1, 2, \dots, Z = 3$] are assumed to be monitored in time (t): the pressure $p_{CSM,in}$ at the inlet of the CSM ($k = 1$), which must not exceed $p_{lim} = 1.8 \text{ MPa}$ (set point at which C2 opens the SVs for the integrity of the joints and headers adjacent to the CSM during quench); the hotspot temperature T_{hs} in the CSM ($k = 2$), which must not exceed the current sharing temperature $T_{cs} = 7.3 \text{ K}$ (if $T > T_{cs}$, electric current starts flowing along copper strands with consequent ohmic heating); the ratio I/I_{cr} between the current flowing in the conductors that wrap the CSM and the critical current ($k = 3$), which must not exceed $(I/I_{cr})_{lim} = 0.5$.

The following partial and complete failure of CP, CV1, CV2, BV, SV1 and SV2 are considered to possibly lead to passing the limits for $p_{CSM,in}$, T_{hs} and I/I_{cr} (Bellaera et al., 2020):

- CP decrease in the rotational speed, leading to a reduction in the mass flow rate at: i) 75%, ii) 50%, iii) 25% or iv) 0% of the nominal value.
- Valves CV1 and CV2 failing: i) stuck open at nominal position; ii) partially closed to a flow area at 50 % of the nominal one; iii) completely closed.
- Valves BV, SV1 and SV2 failing: i) stuck closed at nominal position; ii) partially opened with a flow area of 50 % of the nominal one; iii) completely open.

State vectors of eighteen elements are used to represent any of the 10^8 possible combinations of components states $[m_{CP}, t_{CP}, ord_{CP}, m_{CV1}, t_{CV1}, ord_{CV1}, m_{CV2}, t_{CV2}, ord_{CV2}, m_{BV}, t_{BV}, ord_{BV}, m_{SV1}, t_{SV1}, ord_{SV1}, m_{SV2}, t_{SV2}, ord_{SV2}]$. For the failures, the magnitude (m), the time (t) at which they occur and the order (ord) with respect the other component failures are listed (Bellaera et al., 2020). The *magnitude* (m) is described as follows in the vector:

- The magnitude of the CP is indicated by a discrete value between 0 and 4: if the component is not failed in the considered state vector, $m_{CP} = 0$. Instead, m_{CP} values equal to 1, 2, 3 or 4 correspond to states of reduction of the mass flow rate to 75%, 50%, 25% or 0% of the nominal value, respectively, due to a decrease of its rotational speed.

- The magnitude of valves CV1 and CV2 is indicated by a discrete value between 0 and 3. If the component works correctly, $m = 0$. Instead, if m is equal to 1, 2 or 3, the valve is stuck open, partially closed with a reduction of the flow section area to 50% or completely closed, respectively.
- The magnitude of valves BV, SV1 and SV2 is indicated by a discrete value between 0 and 3, too. If the component is not failed, $m = 0$. Otherwise, if m is equal to 1, 2 or 3, the valve is stuck closed, partially open with flow section area of 50% or completely open, respectively.

The *time* (t) is discretised in six time intervals of 300s each, labelled 1 to 6, corresponding respectively to [0s, 300s], [301s, 600s], [601s, 900s], [901s, 1200s], [1201s, 1500s], [1501s, 1800s]. These indicate the intervals within which the components have occurred. If a value of 0 is indicated for t , this means that the component is not failed.

The *order* (ord) is indicated by a discrete value between 1 and 6: if a component failure order is equal to 1, $ord = 1$, this means that it is the first failure event to occur in time. At the other extreme, if $ord = 6$, then it is the last component failure event. If in a state configuration a component is not failed, its *order* is set to “NaN”.

For instance, a state vector equal to [2, 1, 1, 2, 6, 5, 1, 3, 2, 0, 0, NaN, 1, 3, 3, 3, 5, 4] indicates the failure of the CP in the 1st time interval [0s, 300s] with the flow at 50% of the nominal value, the valves CV2 and SV1 getting stuck at their nominal position during the 3rd time interval [601s, 900s], the complete opening of SV2 in the interval [1201s, 1500s] and the partial closing of CV1 during the last time interval [1501s, 1800s], whereas the BV works correctly.

For any state vector, a simulation by the 4C code can be run to generate the corresponding transient scenario and analyse its outcomes with respect to the LOFA occurrence.

3. PROTOTYPICAL TRANSIENTS IN THE CSM

Among 10^8 state vectors of Section 2, $N_{train} = 83$ have been randomly selected and simulated by the 4C code (Bellaera et al., 2020): this relatively small number has been selected in order to limit the overall

computational cost of the analysis (due to the very high computational time needed for each run: actually, the simulation of one transient takes on average 55 hours on an Intel(R) Xeon(R)TM CPU X5355 @2.66 GHz). The corresponding transient scenarios have been clustered in $C = 9$ "classes" of transients in the CSM (Baraldi et al., 2015; Mandelli et al., 2013; Galushin et al., 2015). Fig.15 , Fig.16 and Fig.17 of Appendix A show the behaviour of $p_{CSM,in}$, T_{hs} and I/I_{cr} (dotted lines) for the N_{train} transients, grouped in the clusters: for each cluster the prototypical transient (i.e., the most representative transient according to a given definite membership to the cluster (Baraldi et al., 2015)) is also plotted (continuous line).

The transient belonging to cluster 4 show the largest values of $p_{CSM,in}$ and T_{hs} , still below the threshold limits p_{lim} and T_{cs} , respectively, whereas the scenarios belonging to clusters 2, 3, 8 and 9 have $p_{CSM,in}$ values lower than the threshold p_0 and none of the scenarios exceed $(I/I_{cr})_{lim}$.

Fig.2 (bottom-left) shows the values of the time $t_{LOFA,C1,i}$ ($i = 1, \dots, N_{train}$), at which the control system C1 detects a LOFA in the i -th scenario, for all the $N_{train} = 83$ scenarios. The LOFA may occur during one of the $Q = 5$ phases of a single pulse of current (Savoldi et al., 2014), represented in Fig.2 (top-left):

- 1) First Magnetization phase (FM): in the first 130s, the current varies from 40 kA to -40 kA in 80s, leading to large AC losses and Eddy currents.
- 2) Burning Phase (B): the current decreases to -45.5 kA for 386s.
- 3) Rump Down phase (R): the current reaches 0 kA at 975s.
- 4) Dwell phase (D): no current flows in the CSM until 1490s (to cool down the CSM after the heat load of the previous phases).
- 5) Last Magnetization phase (M): the current returns to the initial value of 40 kA and, after a plateau of 10s, the pulse starts again for other 1800s.

A matrix $\bar{\mathcal{L}}[C, Q]$ containing the information on LOFA occurrence for each c -th cluster ($c = 1, \dots, C$) at each q -th time interval ($q = 1, \dots, Q$) is built. The generic element $\mathcal{L}_{cq} = 1$ if there is at least one $t_{LOFA,C1,i}$ at the c -th cluster during the q -th phase; otherwise, $\mathcal{L}_{cq} = 0$. Fig.2 (right) shows the map with points for which $\mathcal{L}_{cq} = 1$.

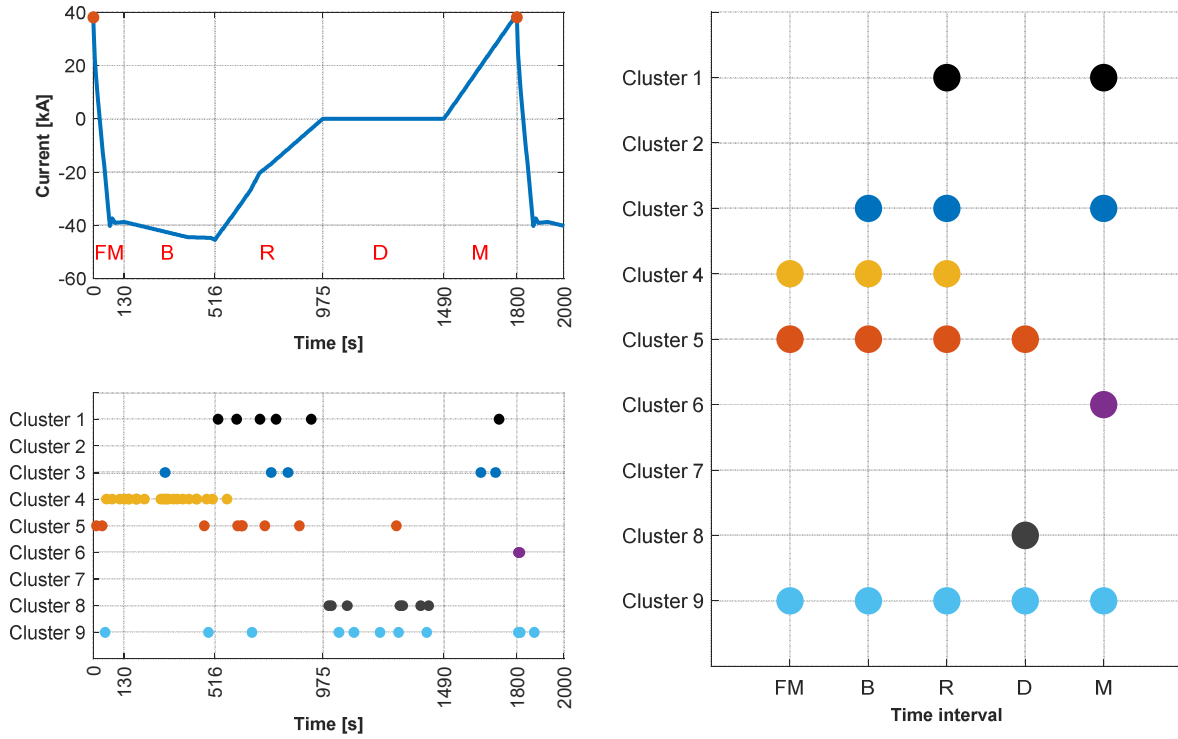


Figure 2 Top, left: single pulse of current in the ITER CSM. Bottom, left: times when LOFA occurs in the 83 (clustered) training scenarios. Right: map of LOFA occurrences in each pulse phase, for each cluster

It can be seen that in the scenarios of cluster 4, LOFA occurs mostly during the early phase of the pulse of current (FM, B, R phases), where AC losses in the CSM are significant, making $p_{CSM,in}$ and T_{hs} reach the largest values, as pointed out before. On the other hand, no LOFAs occur in scenarios of clusters 2 and 7, despite that the components failures that occur in the majority of transients belonging to the two clusters differ between clusters 2 and 7 (only CP failure for cluster 7 vs CP, CV, BV and SV failures for cluster 2), as it can be seen in Fig.3.

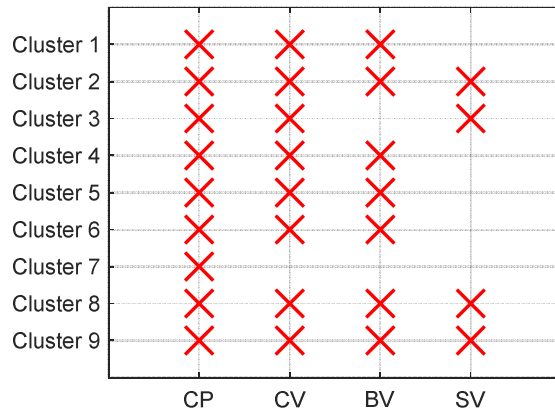


Figure 3 Map of most frequent failures in the clusters

A matrix $\bar{\mathcal{F}}[C, E = 4]$ is built from Fig.3, where each generic element \mathcal{F}_{ce} is referred to the c -th cluster for the e -th component ($e = 1, \dots, E$): the generic element $\mathcal{F}_{ce} = 1$ if the e -th component is a prototypical failure of the c -th cluster; otherwise, $\mathcal{F}_{ce} = 0$.

Notice that failure of the CP is present in all clusters, and that failures of the CV and the BV are present in most of them (except clusters 3 and 7). This shows that the identification of the component failures leading to LOFA (i.e., the LOFA precursors) is difficult if done only from Fig.3. In what follows, we show an approach for an extensive and automatic LOFA precursors identification.

4. ON-LINE SUPERVISED SPECTRAL CLUSTERING FOR LOFA PRECURSORS IDENTIFICATION

An On-line Supervised Spectral Clustering (OSSC) algorithm is trained with the available $N_{train} = 83$ scenarios described in Section 3 and, then, applied to any j -th scenario $x_j^k(t)$ of the remaining $(10^8 - 83)$ scenarios. Each j -th scenario is characterized by $Z = 3$ monitored signals $x_j^k(t)$ ($k = 1, 2$ and 3 correspond to $p_{CSM,in}$, T_{hs} and I/I_{cr} , respectively), whose time evolution emerges from the simulated transient of the cooling circuit in the given state vector configuration.

The OSSC proceeds as follows (further details are reported in Appendix B), for each j -th scenario (the flowchart is sketched in Fig.8 using the FCM approach):

Step 1: The k -th variable trajectory $x_j^k(t)$, $k = 1, 2, 3$, is recorded every time step $\Delta t = 0.01s$ from 0s to 3600s, corresponding to the length of two consecutive current pulses, so $L = 360001$ points for each k -th variable are stored and x_{jl}^k ($l = 1, 2, \dots, L$) is the value of the k -th variable of the j -th scenario at the l -th time step. Each $x_j^k(t)$ trajectory has the same discretization of the $x_i^k(t)$ trajectory and the $\bar{X}^k[N_{train}, L]$ matrix at the i -th row and l -th column contains the value x_{il}^k of the k -th variable of the i -th training scenario at the l -th time point.

Step 2: Each x_{il}^k ($i = 1, 2, \dots, N_{train}; l = 1, 2, \dots, L$) and each x_{jl}^k ($l = 1, 2, \dots, L$) are normalized in the interval $[0.2; 0.8]$ as in Eq.(1):

$$y_{jl}^k = 0.2 + 0.6 \cdot \frac{x_{jl}^k - \min(\bar{X}^k)}{\max(\bar{X}^k) - \min(\bar{X}^k)}, \quad k = 1, \dots, Z \text{ and } l = 1, 2, \dots, L \quad (1)$$

It is worth mentioning that if x_{jl}^k overcomes the maximum (or the minimum) value in \bar{X}^k , y_{jl}^k may not lie in $[0.2; 0.8]$.

Step 3: The Euclidean pointwise distance $\delta_{l,ji}$ between the j -th scenario and the i -th training scenario ($i = 1, 2, \dots, N_{train}$) at the l -th time is calculated as in Eq.(2):

$$\delta_{l,ji} = \sum_{k=1}^Z \sum_{p=1}^l |y_{jp}^k - y_{ip}^k|, \quad i = 1, 2, \dots, N_{train} \text{ and } l = 1, 2, \dots, L \quad (2)$$

Step 4: The similarity vector $\bar{W}_{l,j}[1, N_{train}]$ is built at each l -th time step, whose generic element $w_{l,ji}$ is given in Eq.(3):

$$w_{l,ji} = e^{-F \cdot \delta_{l,ji}^2} \quad \text{with } F = 1.7 \cdot 10^{-9} \text{ (Bellaera et al., 2020)} \quad (3)$$

The higher $w_{l,ji}$, the higher the similarity between the j -th testing scenario and the i -th training scenario until the l -th time step.

Step 5: The row vector $\bar{U}_{l,j}[1, C]$ is calculated projecting $\bar{W}_{l,j}$ in the eigenspace employing Eq.(25) (see Appendix C for the proof). Afterwards, it is normalized determining $\bar{T}_{l,j}[1, C]$, whose generic element $t_{l,jc}$ is given by Eq.(4):

$$t_{l,jc} = \frac{u_{j,jc}}{\sqrt{\sum_{c=1}^C u_{j,jc}^2}}, \quad c = 1, 2, \dots, C \quad (4)$$

Step 6: Each $M_{l,cj}$ membership of the j -th scenario to the c -th cluster at the l -th time step is calculated as in Eq.(5) (which is obtained from Eq.(16) of the FMC algorithm in Appendix B):

$$M_{l,cj} = \left[\sum_{h=1}^C \left(\frac{\|\bar{T}_{l,j} - \bar{A}_c\|}{\|\bar{T}_{l,j} - \bar{A}_h\|} \right)^{\frac{2}{\rho-1}} \right]^{-1}, \quad c = 1, 2, 3, \dots, C \quad (5)$$

where $\bar{A}_c[1, C]$ ($c = 1, 2, \dots, C$) contains the eigenspace coordinates of the prototypical transient of the c -th cluster and $\rho = 2$ is the fuzzy partition exponent (Bezdec, 1981). The membership $M_{l,cj}$ measures the “degree” with which the j -th scenario at the l -th time step “belongs” to the c -th cluster. Fig.4 and Fig.5 show the memberships evolution for a scenario with no failures (hereafter referred to as $j = 0$) and for a scenario with complete closure of CV1 at 623s, respectively: these two scenarios belong to cluster 7 and cluster 5, respectively, because $M_{l,7j}$ in Fig.4 and $M_{l,5j}$ in Fig.5 rapidly rise and reach values close to 1, whereas the other memberships drop gradually to 0.

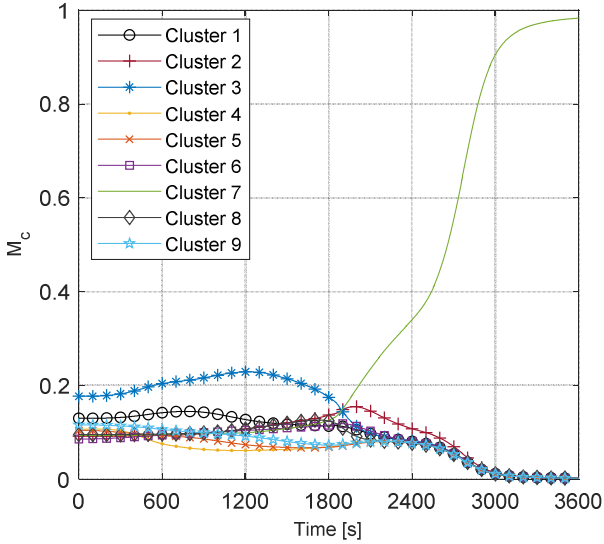


Figure 4 Memberships evolution for a scenario at nominal condition with no failures

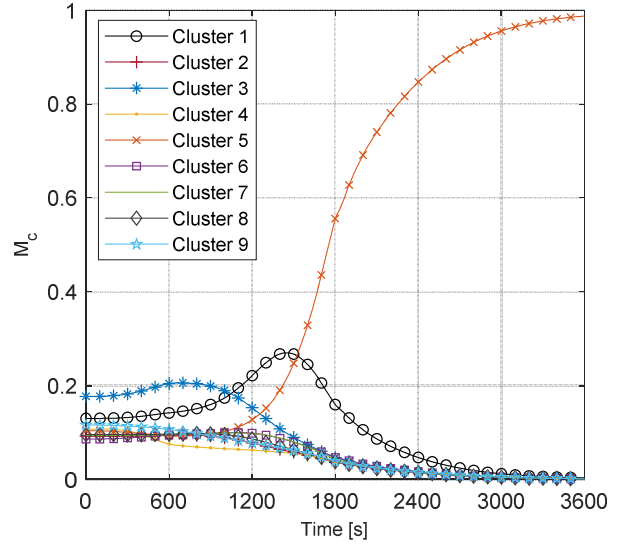


Figure 5 Memberships evolution for a scenario “complete closure of CV1 at 623s” (and $t_{LOFA,C1,j} = 627.14s$)

Step 7: Calculate the pointwise difference between $M_{l,cj}$ and $M_{l,c0}$ resulting in $M_{rel,l,cj}$ (shown by way of example in Fig.6 for the scenario “complete closure of CV1 at 623s”) as in Eq.(6):

$$M_{rel,l,cj} = M_{l,cj} - M_{l,c0} \quad c = 1, 2, \dots, C \quad (6)$$

The difference (6) serves the purpose of “removing” from the membership evolution of the j -th transient to cluster c the “background” contribution of a “standard” scenario at nominal condition with no failures.

Step 8: Calculate $V_{rel,l,cj}$ with Eq.(7), i.e., a discrete estimator of the derivative of the membership $M_{l,cj}$ with respect to the l -th time (shown in Fig.7 for the scenario “complete closure of CV1 at 623s”):

$$V_{rel,l,cj} = \begin{cases} 0 & \text{if } l = 1 \\ \frac{M_{rel,l,cj} - M_{rel,(l-1),cj}}{\Delta t} & \text{if } l \neq 1 \end{cases}, \quad c = 1, 2, \dots, C \quad (7)$$

It is evident from Fig.6 and Fig.7 that $M_{rel,l,cj}$ and $V_{rel,l,cj}$ start deviating from “0” at 623s after the closure of CV1: in particular, the failure of CV1 generates a scenario with an initial affinity to cluster 1 and 5, as testified by the simultaneous increase in the values of $M_{rel,l,1j}$, $M_{rel,l,5j}$, $V_{rel,l,1j}$ and $V_{rel,l,5j}$; however, the increase in $M_{rel,l,5j}$ and $V_{rel,l,5j}$ becomes dominant at about 1450s, correctly and clearly showing that the scenario belongs to cluster 5.

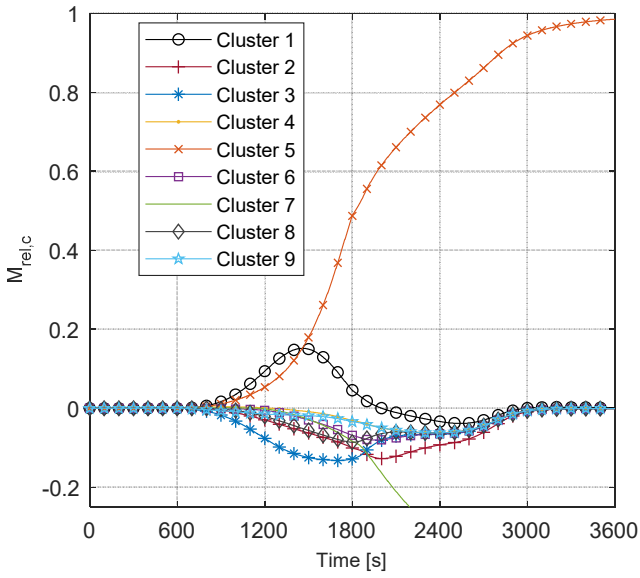


Figure 6 $M_{rel,l,cj}$ evolution for scenario “complete closure of CV1 at 623s”

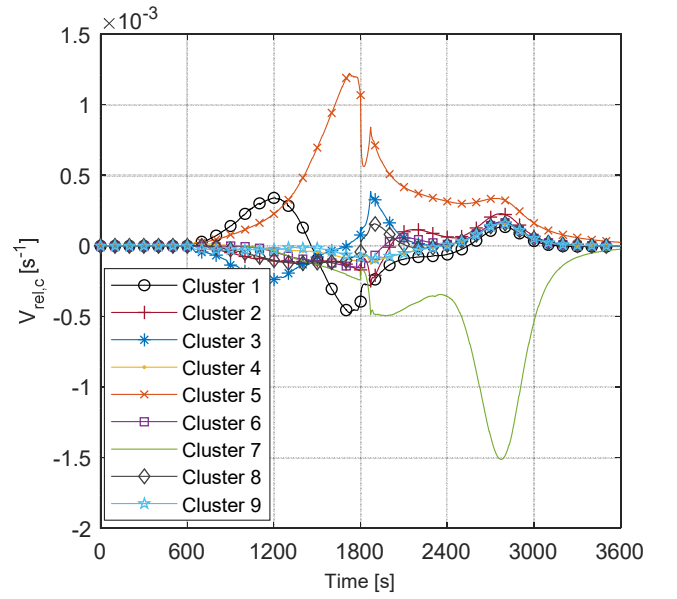


Figure 7 $V_{rel,l,cj}$ evolution for scenario “complete closure of CV1 at 623s”

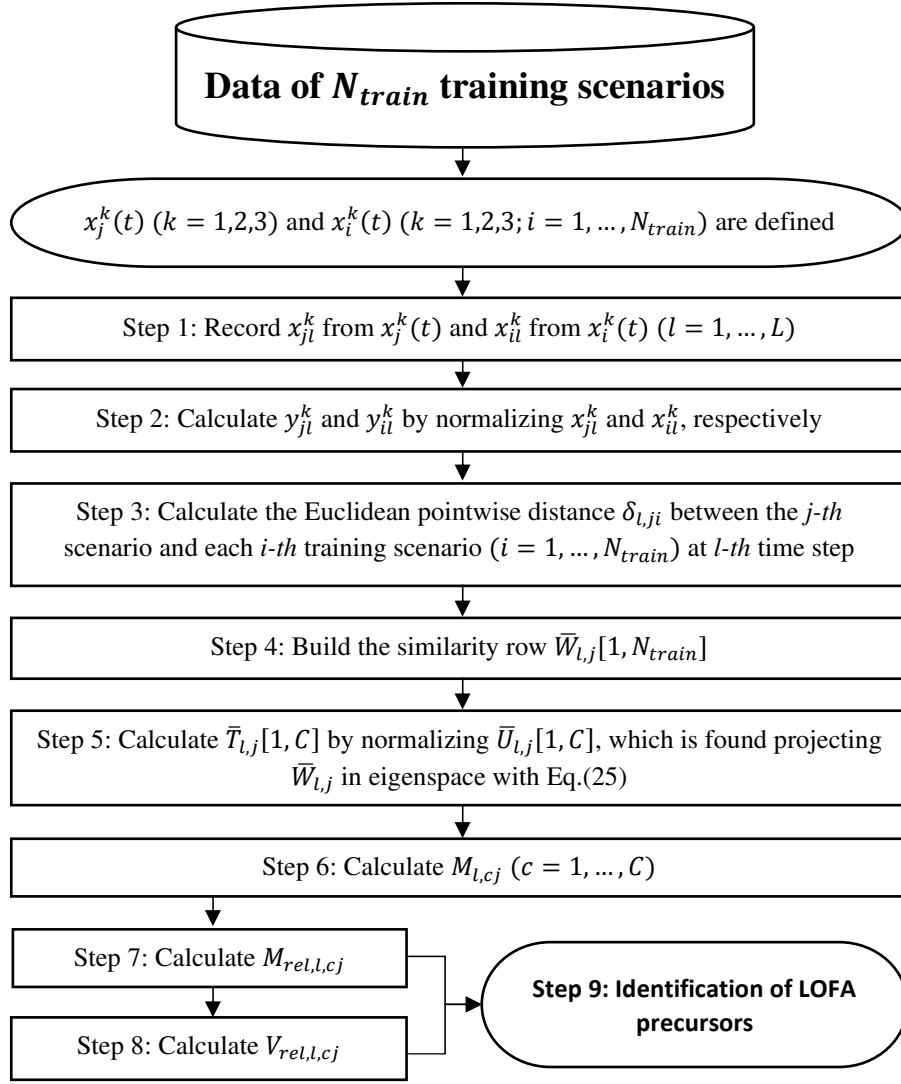


Figure 8 Flow chart of the OSSC procedure

Step 9: Identify LOFA precursors as follows.

Step 9a: Compare $V_{rel,l,cj}$ [$c = 1, \dots, C$] with $V_{lim,LOFA,l}$, following the pseudo-code in Fig.9. In extreme synthesis, if at least two values of $V_{rel,l,cj}$ pass the threshold $V_{lim,LOFA,l}$ (see Fig.10 below) at time l , and if a LOFA can occur in the corresponding clusters (according to the map of Fig.2), the algorithm registers the LOFA precursors.

```

At  $l$ -th time
  Calculate  $V_{1st} = \max_c (V_{rel,l,cj})$ ;
  Calculate  $c_{1st} = \arg \left( \max_c (V_{rel,l,cj}) \right)$ ;
  Calculate  $V_{2nd} = \max_{c \neq c_{1st}} (V_{rel,l,cj})$ ;
  Calculate  $c_{2nd} = \arg \left( \max_{c \neq c_{1st}} (V_{rel,l,cj}) \right)$ ;
   $Flag_{LOFA} = 0$ ;
  If  $(V_{1st} > V_{lim,LOFA,l} \ \& \ V_{2nd} > V_{lim,LOFA,l})$ 
    Find  $q$ -th current phase that corresponds to  $l$ -th time
     $Flag_{LOFA} = \mathcal{L}_{c_{1st}q} * \mathcal{L}_{c_{2nd}q}$ ;    %  $\mathcal{L}_{cq} = \{0,1\}$  (see Section 3 – Fig.2)
  End
  If  $Flag_{LOFA} = 1$ 
    LOFA precursor is identified;
  Else
    LOFA precursor does not exist;
  End

```

Figure 9 Pseudo-code for $V_{rel,l,cj}$ and $V_{lim,LOFA,l}$

The evolution of $V_{lim,LOFA,l}$ is assumed to be that of a monotonic increasing piecewise function that is calculated relying on the information stored in the N_{train} scenarios, following the pseudo-code of Fig.10. The trend of $V_{lim,LOFA,l}$ is initially defined using a discrete set of points obtained from the N_{train} scenarios and joined together to build a stepwise function monotonically increasing.

```

For each  $i$ -th scenario ( $i = 1, \dots, N_{train}$ )
  If LOFA occurs
     $t_{lim,i} = \text{round}((t_{last,Fail,i} + t_{LOFA,C1,i})/2)$ ;
  Else
     $t_{lim,i} = NaN$ ;
  End
End
 $V_{lim,LOFA,l}$  DEFINITION:
Define  $V_{lim,LOFA,1} = 0$ ;
For  $l = 2: 1: L$ 
  Find  $i$  such that  $l$ -th time =  $t_{lim,i}$  ( $i = 1, \dots, N_{train}$ )
  If  $i$  exists
    Calculate  $c_{1st} = \arg(\max_c(V_{rel,l,ci}))$ ;
    Calculate  $V_{lim,i} = \max_{c \neq c_{1st}}(V_{rel,l,ci})$ ;
     $V_{lim,LOFA,l} = V_{lim,i}$ ;
  Else
     $V_{lim,LOFA,l} = V_{lim,LOFA,(l-1)}$ ;
  End
End
 $V_{lim,LOFA,l}$  REVISION:
For  $p = L: -1: 1$ 
  For  $l = 1: 1: (p - 1)$ 
    If  $V_{lim,LOFA,l} > V_{lim,LOFA,p}$ 
       $V_{lim,LOFA,l} = V_{lim,LOFA,p}$ ;
    End
  End
End

```

Figure 10 $V_{lim,LOFA,l}$ calculation procedure

where $t_{last,Fail,i}$ is the time when the last failure before $t_{LOFA,C1,i}$ occurs. Fig.11 reports the results of each step of the procedure in Fig.10.

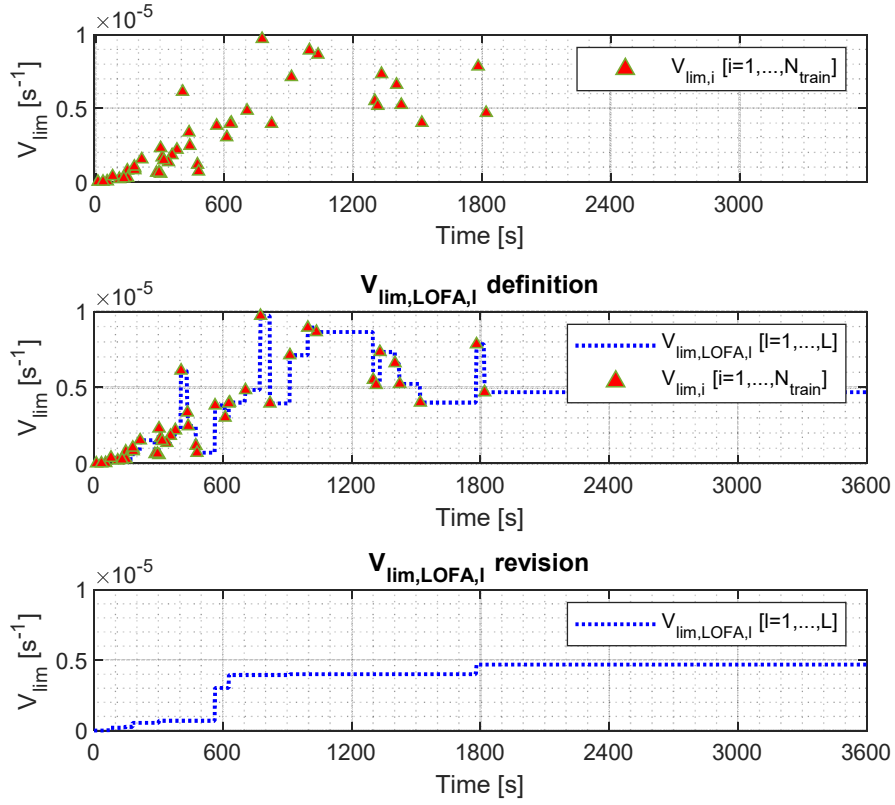


Figure 11 $V_{lim,LOFA,l}$ calculation results

Step 9b: Compare $M_{rel,l,cj}$ ($c = 1, \dots, C$) to the threshold $M_{lim,FAIL,l}(8)$, following the pseudo-code in Fig.12.

In extreme synthesis, if the e -th component is present in all clusters, according to the map of Fig.3, among those where $M_{rel,l,cj}$ exceeds $M_{lim,FAIL,l}$ at the l -th time step, the algorithm identifies the failure of the e -th component as a LOFA precursor.

```

At  $l$ -th time considering an  $e$ -th component
   $Flag_{FAIL,e} = 1$ ;
   $Count_{FAIL,e} = 0$ ;
  For  $c = 1:1:C$ 
    If  $M_{rel,l,cj} > M_{lim,FAIL,l}$ 
       $Flag_{FAIL,e} = Flag_{FAIL,e} * \mathcal{F}_{ce}$ ; %  $\mathcal{F}_{ce} = \{0,1\}$  (see Section 3 – Fig.3)
       $Count_{FAIL,e} = Count_{FAIL,e} + 1$ ;
    End
  End
  If  $Flag_{FAIL,e} = 1$  &  $Count_{FAIL,e} \neq 0$ ;
     $e$ -th component is failed
  Else
     $e$ -th component is not failed;
  End

```

Figure 12 Pseudo-code for $M_{rel,l,cj}$ and $M_{lim,FAIL,l}$

$M_{lim,FAIL,l}$ is calculated as in Eq.(8):

$$M_{lim,FAIL,l} = S \cdot (l^{th} \text{ time}) \quad \text{with } S = 5.56 \times 10^{-8} \text{ s}^{-1} \quad (8)$$

It is worth mentioning that $M_{lim,FAIL,l}$ is assumed to be linearly dependent on time, because δ_{ij} (Eq.10) linearly increases from $t = 0$ to $t = t_{miss} = 3600$ and it is used to calculate $M_{rel,l,cj}$. The value of S is that which maximises the number of training scenarios whose component failures are correctly identified as LOFA precursors, while minimising the time delay between components failures and precursors identification.

5. RESULTS

The proposed procedure has been applied for LOFA precursors identification in $N_{test} = 38$ scenarios, different from the $N_{train} = 83$ scenarios used to build the OSSC method of Section 4. As an example, we show the results with respect to the scenario “complete closure of CV1 at 623s”, whose memberships are plotted in Fig.5 above. In Fig.13 a zoom of the values of each $M_{rel,l,cj}$ and $V_{rel,l,cj}$ ($c = 1, \dots, C$) in the interval [600s,650s] (i.e., when CV1 incidentally fails at 623s) is shown.

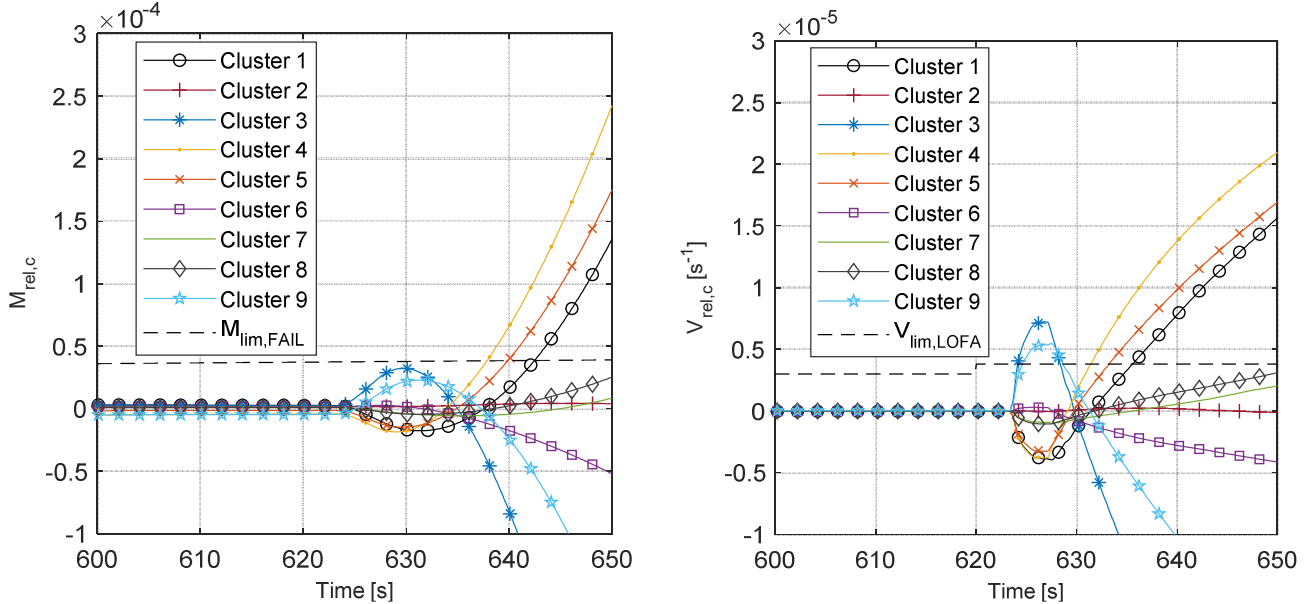


Figure 13 Zoom of $M_{rel,l,cj}$ (left) and $V_{rel,l,cj}$ (right) evolution in the interval [600s-650s] for scenario “complete closure of CV1 at 623s”

It can be seen that $V_{rel,l,3j}$ and $V_{rel,l,9j}$ overcome $V_{lim,LOFA,l}$ at 625s (which is, then, taken as LOFA detection time and plotted with a cross in Fig.14) in the R phase. During this phase of the current pulse, as suggested in Fig.5, the component failures of the prototypical scenarios of clusters 3 and 9 might be responsible for the

LOFA detection during this phase. However, no component is identified as “failed” by the algorithm at that time, because no values of $M_{rel,l,cj}$ have passed the threshold $M_{lim,FAIL,l}$. The threshold value $M_{lim,FAIL,l}$ is reached by $M_{rel,l,4j}$ at 637s, suggesting that component failures of the prototypical transient of cluster 4 (i.e., CP, CV and BV) are responsible (shadowed lines in Fig.14). This is also confirmed when $M_{rel,l,5j}$ and $M_{rel,l,1j}$ overcome $M_{lim,FAIL,l}$ (at 640s and 643s, respectively), since prototypical component failures of clusters 5 and 1 are still CP, CV and BV. In synthesis, the responsible component failures, i.e., the LOFA precursor CV, has been timely and correctly identified.

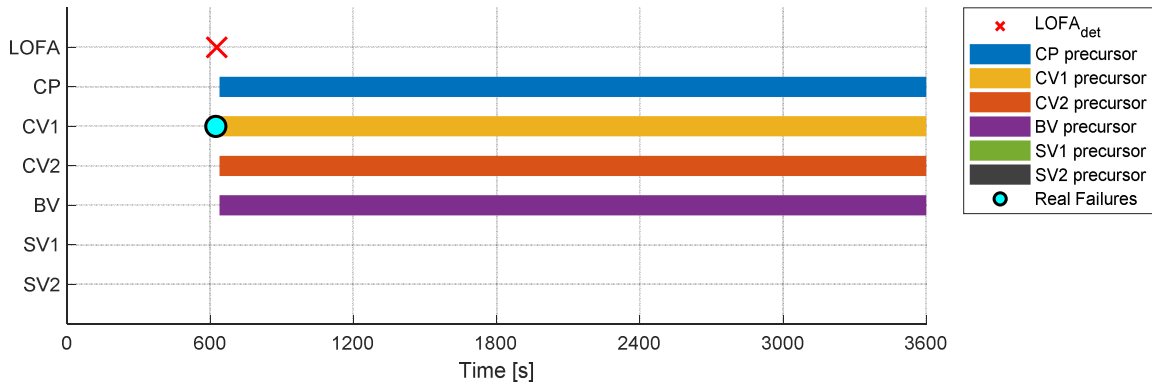


Figure 14 LOFA precursors identification for scenario “complete closure of CV1 at 623s”

In summary, in the present case the LOFA is detected 2s earlier than the actual $t_{LOFA,C1,j}$ whereas the LOFA precursor is identified 10s later than the real malfunctioning of the component, because only a CV is actually failed, whereas CP and BV work correctly. In other words, the number of failed components is slightly overestimated.

In Tab.1, the results of the extensive analysis on the $N_{test} = 38$ scenarios are summarized.

Table 1 Results on $N_{test} = 38$ scenarios

<i>Scenarios with LOFA</i>	32
LOFA predicted in advance	26
LOFA not predicted in advance	6
<i>Scenarios with NO LOFA</i>	6
Correct identification NO LOFA	2
False positive LOFA	4

Among the $N_{test} = 38$ scenarios, in 32 scenarios a LOFA occurs, whereas in 6 it does not. For the former ones, a LOFA is detected in advance, i.e. before $t_{LOFA,C1,j}$, in 26 scenarios. In the 6 scenarios, in which it is not anticipated, the LOFA occurs mainly during the phase D, when no heat is produced by the CSM, and the CSM is not endangered. Also, in 2 of the 6 scenarios in which no LOFA occurs, precursors are identified anyway, whereas in the other 4, LOFA is erroneously detected even though it does not occur (namely, “false positives”).

In Tab.2 the results for the precursor identification of the 32 scenarios with LOFA are presented with respect to:

- Correct precursor identification: the component is failed and correctly identified as precursor.
- False negative: the component is failed, but not identified as precursor.
- Correct identification of normal operation: the component is not failed in the scenario.
- False positive: the component is not failed, but incorrectly identified as precursor.

Table 2 Results of the precursor identification approach for $N_{test} = 38$ scenarios

	<i>Correct precursor identification</i>	<i>False negative</i>	<i>Correct identification of normal operation</i>	<i>False positive</i>
<i>CP</i>	22	1	0	9
<i>CV</i>	18	0	1	13
<i>BV</i>	12	4	1	15
<i>SV</i>	4	1	17	10

It can be seen that most of the precursors are identified correctly by the OSSC algorithm, despite the large number of false positives, that, however, do not endanger the SMCCC, because conservatively overidentifying the failed components.

6. CONCLUSIONS

In this work, an approach is proposed to promptly identify the precursors of a Loss-Of-Flow Accident (LOFA) in the simplified cryogenic cooling circuit (SMCCC) of ITER Central Solenoid (CS) module. In case of a LOFA, cooling is compromised, and pressure and temperature inside the CS may surge rapidly. An On-line Supervised Spectral Clustering (OSSC) method is developed, making use of the Fuzzy C-Means (FCM)

algorithm to identify LOFA precursors. A simulated case study has been considered, using the deterministic 4C code to mimic the SMCCC behaviour for $N_{train} = 83$ components failures scenarios of training and additional $N_{test} = 38$ scenarios to verify the effectiveness of the method. The results obtained show that the method proposed timely recognises LOFA precursors and identifies most of the components failed. On the other hand, it erroneously detects LOFA precursors in some scenarios with no LOFA and identifies as precursors some components that are not actually failed. These errors are on the conservative side but may reduce availability, due, e.g., to unnecessary inspections following the precursors identification.

The over-identification may be reduced by improving the quality of the maps used for LOFA precursors identification with more simulations. To reduce the computational cost of the simulations one way is to resort to a metamodel to emulate the 4C code.

APPENDIX A – Nine clusters of the N_{train} scenarios

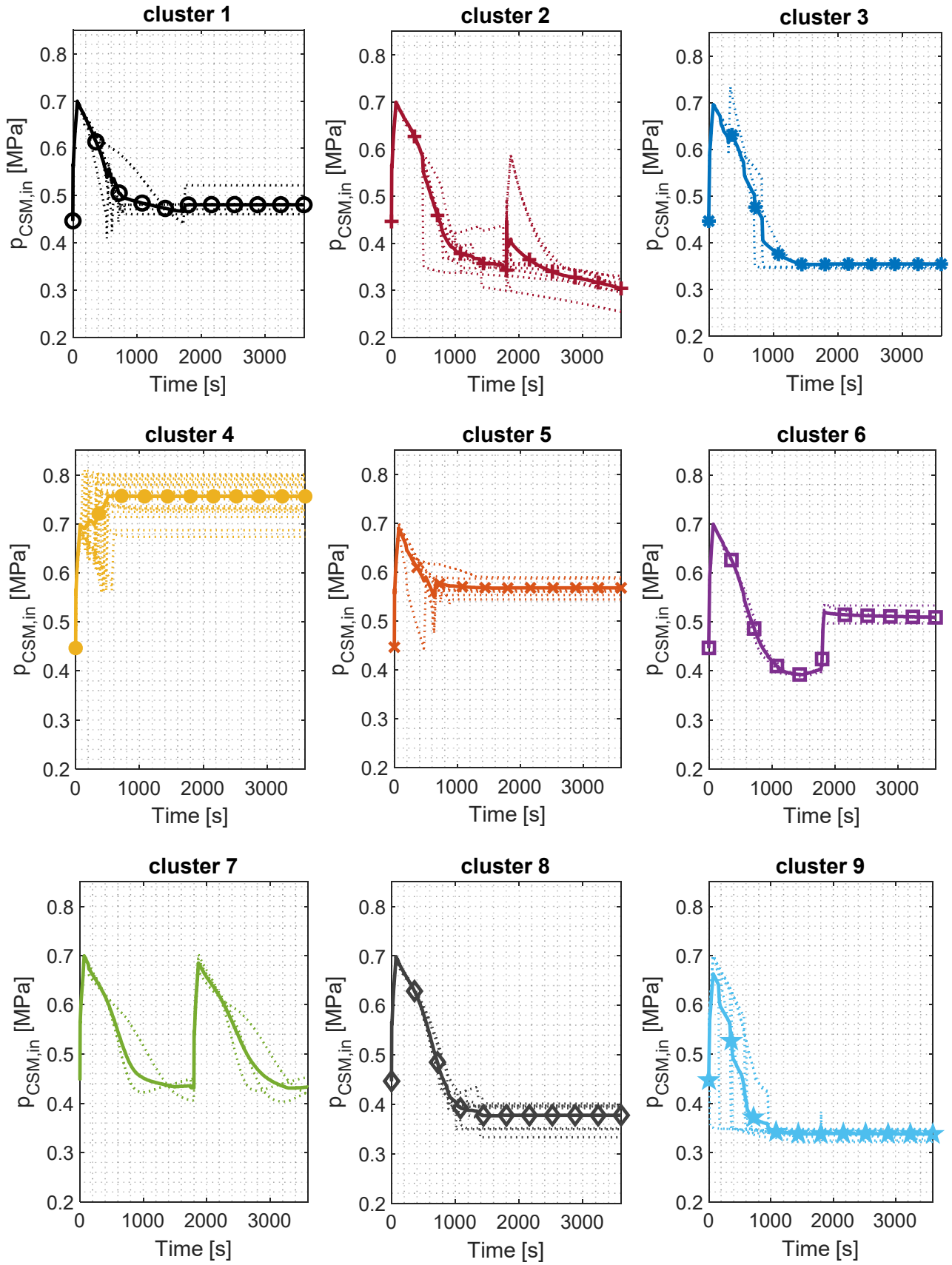


Figure 15 Nine clusters of $p_{CSM,in}$ transient scenarios

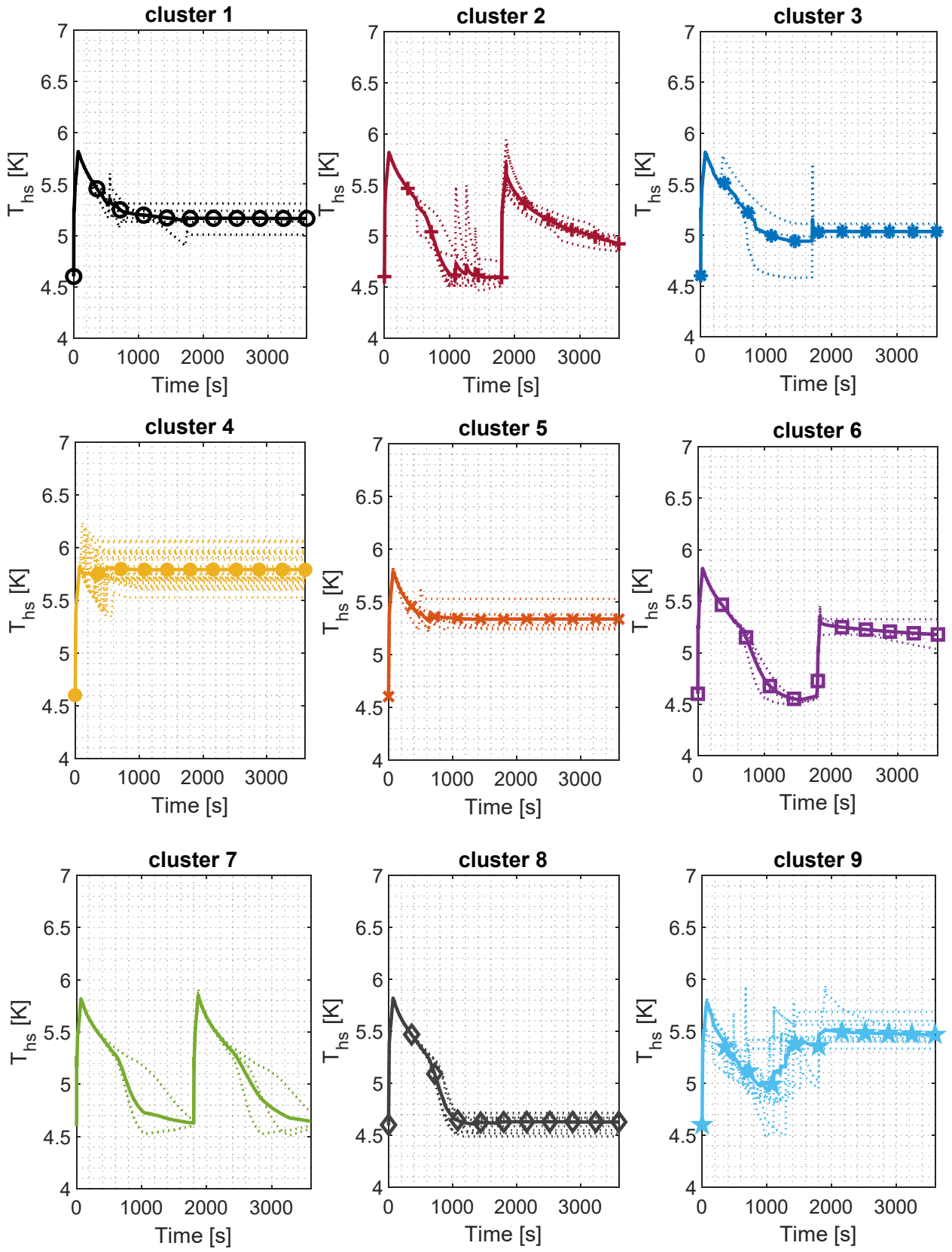


Figure 16 Nine clusters of T_{hs} transient scenarios

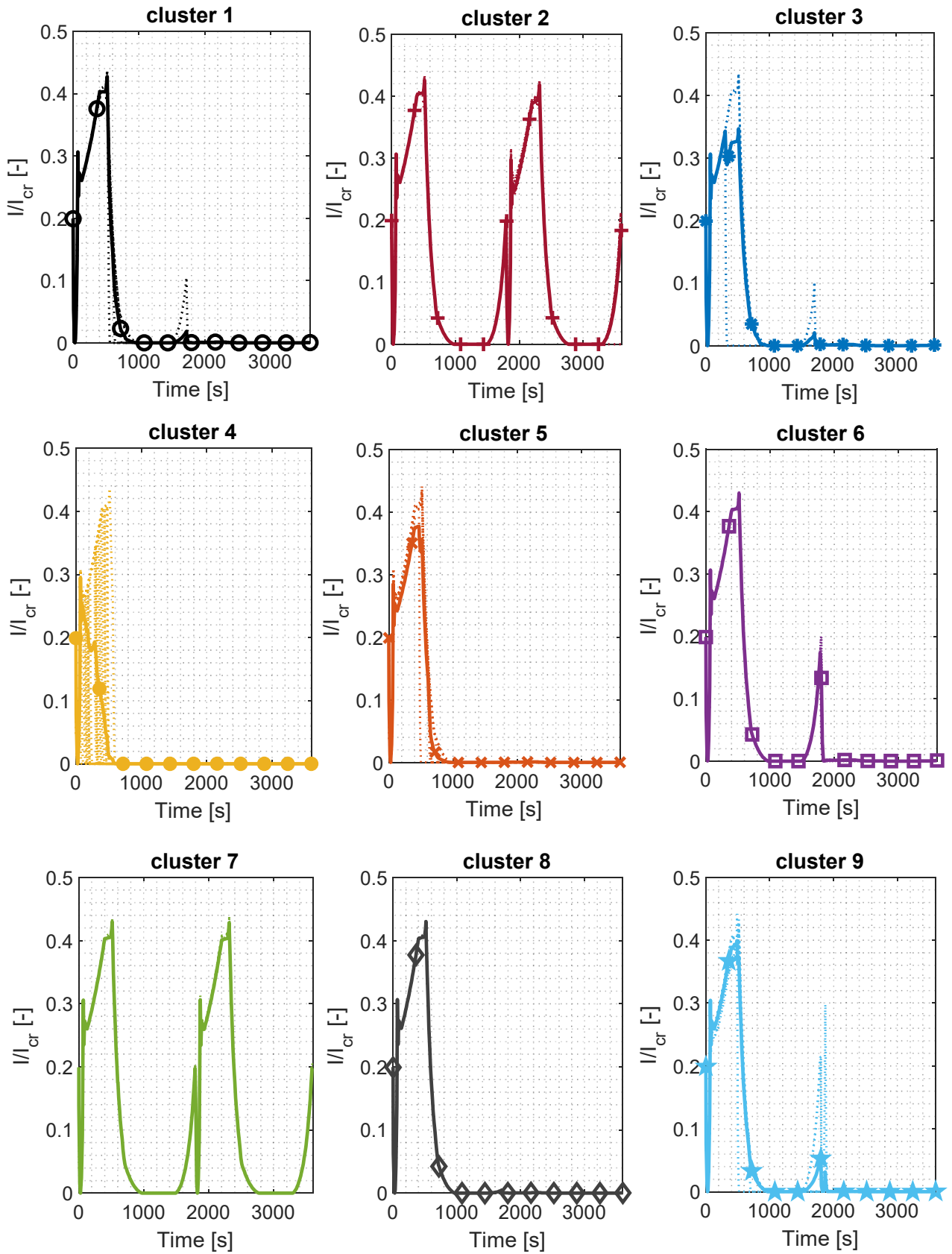


Figure 17 Nine clusters of I/I_{cr} transient scenarios

APPENDIX B – Spectral Clustering embedding the Fuzzy C-Means

Spectral Clustering (SC) lets N objects to be classified in C clusters through a similarity measure w between them (Bellaera et al., 2020; Von Luxburg, 2007). In this case, each similarity value is calculated using $Z = 3$ trajectories, representing $p_{CSM,in}(k = 1)$, $T_{hs}(k = 2)$ and $I/I_{cr}(k = 3)$, of L time steps and collected in the similarity matrix $\bar{\bar{W}}[N, N]$ from which the Normalized Laplacian matrix $\bar{\bar{L}}_{sym}$ is calculated. Features needed to classify the N objects are extracted from $\bar{\bar{L}}_{sym}$ and fed to the Fuzzy C-Means (FCM) code, which proceeds according to the following steps (Baraldi et al., 2013):

Step 1: The matrix $\bar{\bar{X}}^k[N, L]$ is built for each k -th variable considered, containing in the rows the N transients of L time steps of that variable and its generic element is $x_{il}^k (i = 1, 2, \dots, N; l = 1, 2, \dots, L)$ referring to the i -th scenario at the l -th time.

Step 2: Each $x_{il}^k (i = 1, 2, \dots, N; l = 1, 2, \dots, L)$ is normalized in the interval $[0.2, 0.6]$, determining y_{il}^k as in Eq.(9):

$$y_{il}^k = 0.2 + 0.6 \cdot \frac{x_{il}^k - \min(\bar{\bar{X}}^k)}{\max(\bar{\bar{X}}^k) - \min(\bar{\bar{X}}^k)}, \quad k = 1, \dots, Z \quad (9)$$

Step 3: The Euclidean pointwise distance δ_{ij} between an i -th object and a j -th one ($j = 1, 2, \dots, N$) is determined as in Eq.(10):

$$\delta_{ij} = \sum_{k=1}^Z \sum_{l=1}^L |y_{il}^k - y_{jl}^k| \quad (10)$$

Step 4: The generic element w_{ij} of the similarity matrix $\bar{\bar{W}}[N, N]$ is obtained from δ_{ij} as follows in Eq.(11) (Joentgen et al., 1999; Dubois et al., 1988):

$$w_{ij} = e^{-\left(\frac{\ln(\alpha)}{\beta} \delta_{ij}^2\right)} = e^{-F \cdot \delta_{ij}^2} \quad (11)$$

The Higher the value of $-\ln(\alpha)/\beta$ is, the closer are the N objects and more enhanced the similarity between them (Baraldi et al., 2013) [$F = -\ln(\alpha)/\beta$ is set to $1.7 \cdot 10^{-9}$]. w_{ij} can assume a value between 0 and 1: if it is close to 1, the i -th and the j -th objects considered are very similar; instead, if it is near to 0, the two objects

are very different. Consequently, each element of the matrix $\bar{\bar{W}}$ in the diagonal is equal to 1, because $\delta_{ii} = 0$.

This matrix is also symmetrical, because $\delta_{ij} = \delta_{ji}$.

Step 5: Each element $d_i (i = 1, \dots, N)$ of the Degree matrix $\bar{\bar{D}}[N, N]$, which is a diagonal matrix, is determined with Eq.(12):

$$d_i = \sum_{j=i}^N w_{ij} \quad (12)$$

Now, it is possible to calculate the Laplacian matrix $\bar{\bar{L}}[N, N]$ by subtracting the Similarity matrix to the Degree matrix: $\bar{\bar{L}} = \bar{\bar{D}} - \bar{\bar{W}}$.

Step 6: The Normalized Laplacian matrix $\bar{\bar{L}}_{sym}[N, N]$ is computed normalizing $\bar{\bar{L}}$ as in Eq.(13):

$$\bar{\bar{L}}_{sym} = \bar{\bar{D}}^{-1/2} \bar{\bar{L}} \bar{\bar{D}}^{-1/2} = \bar{\bar{I}} - \bar{\bar{D}}^{-1/2} \bar{\bar{W}} \bar{\bar{D}}^{-1/2} \quad (13)$$

Step 7: The C smallest eigenvalues $\lambda_1, \lambda_2, \dots, \lambda_C$ and their associated eigenvectors $\vec{u}_1, \vec{u}_2, \dots, \vec{u}_C$ of the matrix $\bar{\bar{L}}_{sym}$ are extracted. All the eigenvalues are between 0 and 1, with 0 included, and those stored are very small compared to λ_{C+1} .

Step 8: The matrix $\bar{\bar{U}}[N, C]$ is made associating to each c -th column the $\vec{u}_c[N, 1]$ eigenvector obtained by the previous phase. Afterward, this matrix is normalized calculating the matrix $\bar{\bar{T}}[N, C]$, whose generic element t_{ic} is determined as follows in Eq.(14):

$$t_{ic} = \frac{u_{ic}}{\sqrt{\sum_{c=1}^C u_{ic}^2}}, \quad i = 1, 2, \dots, N, \quad c = 1, 2, \dots, C \quad (14)$$

The eigenspace coordinates of the object i -th are contained in each row i -th of the matrix $\bar{\bar{T}}$, so $\bar{\bar{T}}_i = [t_{i1}, t_{i2}, \dots, t_{iC}]$ is the vector that contains these coordinates.

Step 9: The matrix $\bar{\bar{T}}$, which contains the features extracted of the N objects, is fed to the FCM code to cluster them in C groups.

At the end of this phase, two matrices are generated (Bezdec, 1981):

- A matrix $\bar{\bar{\mathcal{A}}}[C, C]$, containing in each c -th row the eigenspace coordinates of the centre of the c -th cluster, so $\bar{A}_c = [a_{c1}, a_{c2}, \dots, a_{cC}]$ is the vector that contains these coordinates.
- A matrix $\bar{\bar{\mathcal{M}}}[C, N]$ whose generic element is the M_{ci} membership degree of the i -th object for the c -th cluster; then, the i -th object is assigned to belong to the cluster with the highest membership and/or with the membership above a certain limit (e.g. $M_{lim} = 0.7$).

The FCM code follows different steps (Alata et al., 2008):

- I. Each M_{ci} is initialized with a random value between 0 and 1 and each column of $\bar{\bar{\mathcal{M}}}$ is normalized: the rule $\sum_{c=1}^C M_{ci} = 1$ must be satisfied.
- II. The matrix $\bar{\bar{\mathcal{M}}}$ is used to determine the centres of the C clusters as in Eq.(15):

$$\bar{A}_c = \frac{\sum_{i=1}^N M_{ci}^\rho \bar{T}_i}{\sum_{i=1}^N M_{ci}^\rho}, \quad c = 1, 2, \dots, C \quad (15)$$

The parameter ρ is the fuzzy partition exponent (Bezdec, 1981) and it is higher than 1: normally it is set to 2. In this way, memberships with higher values play a stronger weight in the averaging formula of Eq.(15).

- III. All the memberships are recalculated as in Eq.(16):

$$M_{ci} = \frac{1}{\sum_{h=1}^C \left(\frac{\|\bar{T}_i - \bar{A}_c\|}{\|\bar{T}_i - \bar{A}_h\|} \right)^{\frac{2}{\rho-1}}} \quad (16)$$

- IV. The objective function J_m is determined and reduced at each iteration, as in Eq.(17):

$$J_m = \sum_{i=1}^N \sum_{c=1}^C M_{ci}^\rho \|\bar{T}_i - \bar{A}_c\|^2 \quad (17)$$

The minimum improvement between each step is usually set equal to 10^{-5} ; if this value is not reached, the algorithm is repeated from ii to iv until J_m is improved.

Step from ii to iv are iterated more times in order to minimize the objective function J_m . Normally, 100 iterations are set for the optimization, in the case study presented in this paper.

APPENDIX C – Supervised Spectral Clustering: Projection in eigenspace

In OSSC, it is essential to reprocess the j -th scenario in the $\bar{T}_{l,j}[1, C]$ eigenspace coordinates at the l -th time, because each $\bar{A}_c[1, C]$ center of the c -th cluster, employed to determine each membership $m_{l,cj}$ ($l = 1, \dots, L; c = 1, \dots, C$) of the j -th scenario to the c -th cluster at l -th time as in Eq.(5), is found minimizing the objective function J_m of Eq.(17) using the eigenspace coordinates $\bar{T}_i[1, C]$ ($i = 1, \dots, N_{train}$) of the $N_{train} = 83$ training scenarios. Therefore, a relation between the $\bar{W}_{l,j}[1, N_{train}]$ similarity vector, containing the similarity between the j -th scenario and each i -th training scenario, and $\bar{U}_{l,j}[1, C]$, from which $\bar{T}_{l,j}[1, C]$ is obtained with Eq.(4), must be found, because we cannot proceed like in Appendix B building a Laplacian matrix from $\bar{W}_{l,j}$ in order to discover its eigenvectors and proceed with the analysis.

Anyway, it could be complex finding the relation between $\bar{W}_{l,j}$ and $\bar{U}_{l,j}$, so it is better to find for a single row: this relation between \bar{W}_i and \bar{U}_i , i.e., the i -th rows of \bar{W} and \bar{U} respectively, can, then be used for a new scenario.

We start from the relation between a λ_c ($c = 1, \dots, C$) eigenvalue and its associated $\vec{u}_c[N_{train}, 1]$ eigenvector of the normalized Laplacian matrix \bar{L}_{sym} , which is a squared matrix, expressed in Eq.(18):

$$\bar{L}_{sym} \vec{u}_c = \lambda_c \vec{u}_c \quad (18)$$

This last matrix could be rewritten using Eq.(13).

$$(\bar{I} - \bar{D}^{-1/2} \bar{W} \bar{D}^{-1/2}) \vec{u}_c = \lambda_c \vec{u}_c \quad (19)$$

$\bar{D}[N_{train}, N_{train}]$ is a diagonal matrix and each term of the diagonal is calculated from \bar{W} using Eq.(12), whereas $\bar{I}[N_{train}, N_{train}]$ is an identity matrix.

With some calculation from Eq.(19), we find:

$$\vec{u}_c - \bar{D}^{-1/2} \bar{W} \bar{D}^{-1/2} \vec{u}_c = \lambda_c \vec{u}_c \quad (20)$$

$$(1 - \lambda_c) \vec{u}_c = \bar{D}^{-1/2} \bar{W} \bar{D}^{-1/2} \vec{u}_c \quad (21)$$

Finally, a relation between \bar{W} matrix and a \vec{u}_c eigenvector, which is a column of \bar{U} , is expressed in Eq.(22):

$$\vec{u}_c = \frac{1}{1 - \lambda_c} \bar{\bar{D}}^{-1/2} \bar{\bar{W}} \vec{P}_c \quad c = 1, 2, \dots, C \quad (22)$$

$$\text{with} \quad \vec{P}_c = \bar{\bar{D}}^{-1/2} \vec{u}_c \quad (23)$$

Therefore, it is possible to obtain all the $\bar{\bar{U}}$'s columns from Eq.(22) knowing $\bar{\bar{W}}$, $\bar{\bar{D}}$, \vec{P}_c and $\lambda_c (c = 1, \dots, C)$.

Eq.(22) could be generalized to find a single element u_{ic} of the matrix $\bar{\bar{U}}$, using a single row $\bar{\bar{W}}_i$ of the similarity matrix $\bar{\bar{W}}$, as in Eq.(24):

$$u_{ic} = \frac{d_i^{-1/2}}{1 - \lambda_c} \bar{\bar{W}}_i \vec{P}_c \quad c = 1, 2, \dots, C \quad (24)$$

In this way, the row $\bar{\bar{U}}_i$ can be found iterating Eq.(24) for all the λ_c eigenvalues and its \vec{P}_c vectors, from Eq.(23).

Adapting Eq.(24) for the $\bar{\bar{W}}_{l,j}$ similarity vector of the new j -th scenario at the l -th time, Eq.(25) is obtained:

$$u_{l,jc} = \frac{d_{l,j}^{-1/2}}{1 - \lambda_c} \bar{\bar{W}}_{l,j} \vec{P}_c \quad c = 1, 2, \dots, C \quad (25)$$

$$\text{with} \quad d_{l,j} = \sum_{i=1}^{N_{train}} w_{l,ji} \quad (26)$$

$\bar{\bar{U}}_{l,j}$ is calculated repeating Eq.(25) for each λ_c and \vec{P}_c from $c = 1$ to $c = C$.

REFERENCES

- (Alata et al., 2008) Alata, M., Molhim, M., Ramini, A., 2008. Optimizing of Fuzzy C-Means Clustering. World Acad. Sci. Eng. Technol. 2, 224–229.
- (Al-Dahidi et al., 2018) Al-Dahidi, S., Di Maio, F., Baraldi, P., Zio, E., Seraoui, R., 2018, A framework for reconciliating data clusters from a fleet of nuclear power plants turbines for fault diagnosis, Applied Soft Computing, Volume 69, Pages 213-231, ISSN 1568-4946, <https://doi.org/10.1016/j.asoc.2018.04.044>.
- (Baraldi et al., 2015) Baraldi, P., Di Maio, F., Rigamonti, M., Zio, E., Seraoui, R., 2015, Clustering for unsupervised fault diagnosis in nuclear turbine shut-down transients, Mechanical Systems and Signal Processing, Volumes 58–59, Pages 160-178, ISSN 0888-3270, <https://doi.org/10.1016/j.ymssp.2014.12.018>.
- (Baraldi et al., 2013) Baraldi, P., Di Maio, F., Zio, E., 2013, Unsupervised Clustering for Fault Diagnosis in Nuclear Power Plant Components, International Journal of Computational Intelligence Systems, 6, 764-777, 10.1080/18756891.2013.804145.
- (Bellaera et al., 2020) Bellaera, R., Bonifetto, R., Di Maio, F., Pedroni, N., Savoldi, L., Zanino, R., Zio, E., 2020, "Integrated Deterministic and Probabilistic Safety Assessment of a Superconducting Magnet Cryogenic Cooling Circuit for Nuclear Fusion

Applications", Reliability Engineering & System Safety, Volume 201, 106945, ISSN 0951-8320, <https://doi.org/10.1016/j.res.2020.106945>

(Bezdec, 1981) Bezdec, J.C., 1981, Pattern Recognition with Fuzzy Objective Function Algorithms, Plenum Press, New York.

(Bigot, 2018) Bigot, B., 2018, ITER construction and manufacturing progress toward first plasma, Fusion Engineering and Design, ISSN 0920-3796, <https://doi.org/10.1016/j.fusengdes.2018.11.052>

(Di Maio et al., 2016) Di Maio, F., Vagnoli, M., Zio, E., 2016, Transient identification by clustering based on Integrated Deterministic and Probabilistic Safety Analysis outcomes, Annals of Nuclear Energy, Volume 87, Part 2, Pages 217-227, ISSN 0306-4549, <https://doi.org/10.1016/j.anucene.2015.09.007>.

(Dubois et al., 1988) Dubois, D., Prade, H., Testemale, C., 1988. Weighted Fuzzy Pattern Matching. Fuzzy Sets Syst. 28, 313–331. [https://doi.org/10.1016/0165-0114\(88\)90038-3](https://doi.org/10.1016/0165-0114(88)90038-3).

(Galushin et al., 2015) Galushin, S., Kudinov, P., 2015. Scenario Grouping and Classification Methodology for Postprocessing of Data Generated by Integrated Deterministic-Probabilistic Safety Analysis. Science and Technology of Nuclear Installations, Article ID 278638, 13 pages, <http://dx.doi.org/10.1155/2015/278638>.

(IAEA, 2002) IAEA, 2002, ITER Technical Basis, ITER EDA Documentation Series No. 24, IAEA, Vienna

(ITER, 2018) ITER - the way to new energy [Online]. - November 30, 2018. - <http://www.iter.org/>

(ITER, 2006) ITER_D_22HV5L v2.2, 2006 ITER: Design Description Document: DDD 11 Magnet

(ITER, 2009) ITER_D_2NBKXY v1.2, 2009. ITER Design Description Document: Magnets – Conductors, 09/09/2009.

(ITER, 2014) ITER_D_K7G8GN v2.1, 2014. Central Interlock System Strategy for ITER Magnet Protection: Machine Protection Functions, January 24, 2014.

(Joentgen et al., 1999) Joentgen, A., Mikenina, L., Weber, R., Zimmermann, H.-J., 1999. Dynamic fuzzy data analysis based on similarity between functions. Fuzzy Sets Syst. 105, 81–90. [https://doi.org/10.1016/S0165-0114\(98\)00337-6](https://doi.org/10.1016/S0165-0114(98)00337-6)

(Mandelli et al., 2013) Mandelli, D., Smith, C., Yilmaz, A., Aldemir, T., 2013. Mining nuclear transient data through symbolic conversion. Int. Top. Meet. Probabilistic Saf. Assess. Anal. 2013, PSA 2013 3.

(Mitchell et al., 2008) Mitchell, N., Bessette, D., Gallix, R., Jong, C., Knaster, J., Libeyre, P., Sborchia, C., Simon, F. 2008. The ITER magnet system. IEEE Trans. Appl. Supercond. 18: 435–440.

(Savoldi et al., 2014) Savoldi, L., Bonifetto, R., Carli, S., Froio, A., Foussat, A., Zanino, R., 2014, Artificial Neural Network (ANN) modelling of the pulsed heat load during ITER CS magnet operation, Cryogenics, Volume 63, Pages 231-240, ISSN 0011-2275, <https://doi.org/10.1016/j.cryogenics.2014.03.003>

(Savoldi et al., 2018) Savoldi, L., Bonifetto, R., Pedroni, N., Zanino, R. 2018. Analysis of a protected Loss Of Flow Accident (LOFA) in the ITER TF coil cooling circuit. IEEE Transactions on Applied Superconductivity 28(3): 4202009.

(Savoldi et al., 2010) Savoldi, L., R., Casella, F., Fiori, B., Zanino, R. 2010. The 4C Code for the Cryogenic Circuit Conductor and Coil modelling in ITER, Volume 50, Issue 3, Pages 167-176, ISSN 0011-2275, <https://doi.org/10.1016/j.cryogenics.2009.07.008>

(Takahashi et al., 2006) Takahashi, Y., Yoshida, K., Nabara, Y., Edaya, M. and Mitchell, N., June 2006, "Simulation of Quench Tests of the Central Solenoid Insert Coil in the ITER Central Solenoid Model Coil," in IEEE Transactions on Applied Superconductivity, vol. 16, no. 2, pp. 783-786. doi: 10.1109/TASC.2006.873254

(Von Luxburg, 2007) Von Luxburg, U., 2007, A tutorial on spectral clustering, Stat. Comput. 17, 395–416. <https://doi.org/10.1007/s11222-007-9033-z>

(Wu et al., 2016) Wu, Y., Chen, Z., Hu, L., Jin, M., Li, Y., Jiang, J., Yu, J., Alejaldre, C., Stevens, E., Kim, K., Maisonnier, D., Kalashnikov, A., Tobita, K., Jackson, D., Perrault, D., 2016. Identification of safety gaps for fusion demonstration reactors. Nat. Energy 1, 16154.

(Zanino et al., 2010) Zanino, R., Bessette, D., Savoldi, L., R., 2010, Quench analysis of an ITER TF coil, Fusion Engineering and Design, Volume 85, Issue 5, Pages 752-760, ISSN 0920-3796, <https://doi.org/10.1016/j.fusengdes.2010.04.056>.